

# Journal of Materials Chemistry C

Accepted Manuscript



This is an *Accepted Manuscript*, which has been through the Royal Society of Chemistry peer review process and has been accepted for publication.

*Accepted Manuscripts* are published online shortly after acceptance, before technical editing, formatting and proof reading. Using this free service, authors can make their results available to the community, in citable form, before we publish the edited article. We will replace this *Accepted Manuscript* with the edited and formatted *Advance Article* as soon as it is available.

You can find more information about *Accepted Manuscripts* in the [Information for Authors](#).

Please note that technical editing may introduce minor changes to the text and/or graphics, which may alter content. The journal's standard [Terms & Conditions](#) and the [Ethical guidelines](#) still apply. In no event shall the Royal Society of Chemistry be held responsible for any errors or omissions in this *Accepted Manuscript* or any consequences arising from the use of any information it contains.

# An efficient blue-emitting $\text{Sr}_5(\text{PO}_4)_3\text{Cl}:\text{Eu}^{2+}$ phosphor for the application in near-UV white light-emitting diodes

Jianghui Zheng<sup>1</sup>, Qijin Cheng<sup>1</sup>, Shunqing Wu<sup>2</sup>, Ziquan Guo<sup>3</sup>, Yixi Zhuang,<sup>4</sup> Yijun Lu<sup>3</sup>, Ye Li<sup>4</sup> and Chao Chen<sup>1,2,3\*</sup>

<sup>1</sup>School of Energy Research, Xiamen University, Xiamen 361005, China

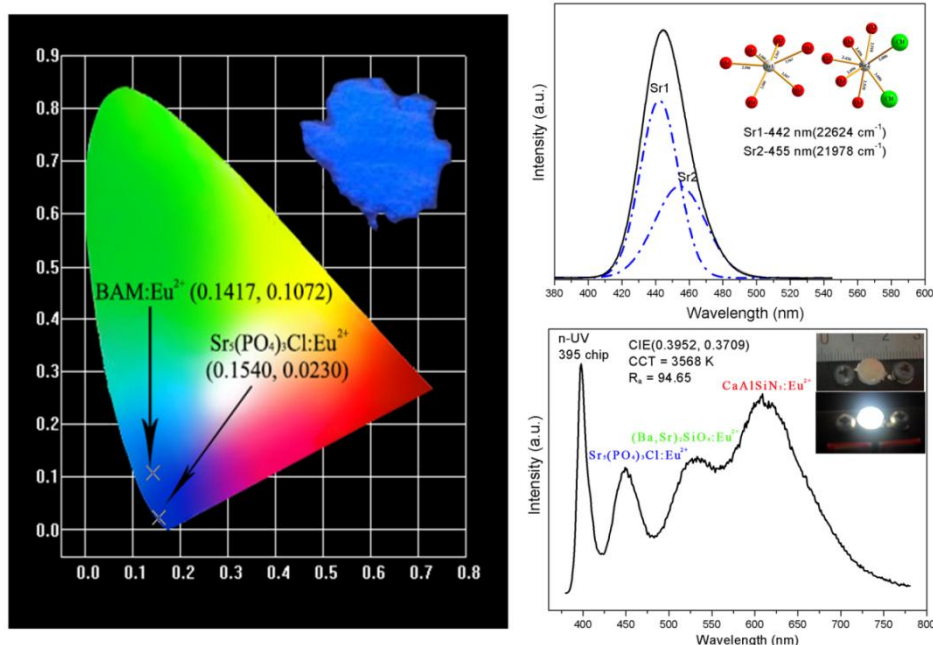
<sup>2</sup>Department of Physics, Xiamen University, Xiamen, 361005, China

<sup>3</sup>Department of Electronic Science, Fujian Engineering Research Center for Solid-state Lighting, Xiamen University, Xiamen, 361005, China

<sup>4</sup>College of Materials, Xiamen University, Xiamen, 361005, China

## Text and Figure for Table of Contents

It is demonstrated that  $\text{Eu}^{2+}$  doped  $\text{Sr}_5(\text{PO}_4)_3\text{Cl}$  blue-emitting phosphors (prepared by conventional high temperature solid-state reactions) feature good thermal ability, high color purity and can be efficiently excited by near-UV light. Particularly, the warm w-LED device based on the phosphors has a high color-rendering index ( $R_a = 94.65$ ) at a correlated color temperature of 3567.84 K with CIE coordinates of (0.3952, 0.3709).



\* Corresponding author Tel. /fax: +86 592 2182458.  
E-mail address: cchen@xmu.edu.cn.

### Summary

A series of  $\text{Eu}^{2+}$  doped  $\text{Sr}_5(\text{PO}_4)_3\text{Cl}$  blue-emitting phosphors was prepared by conventional high-temperature solid-state reactions. The crystal structure, electronic structure, reflectance spectra, thermal stability and quantum efficiency of the  $\text{Sr}_5(\text{PO}_4)_3\text{Cl}:\text{Eu}^{2+}$  phosphor, as well as its application in white near-UV light-emitting diodes have been investigated. The optimization of the lattice parameters and the electronic structure of  $\text{Sr}_5(\text{PO}_4)_3\text{Cl}$  host matrix have been calculated based on density functional theory (DFT). The crystal structure of  $\text{Sr}_5(\text{PO}_4)_3\text{Cl}:\text{Eu}^{2+}$  was confirmed by X-ray diffraction. The concentration quenching of  $\text{Eu}^{2+}$  ions in the  $\text{Sr}_5(\text{PO}_4)_3\text{Cl}$  host is determined to be 1.0 mol% and the physical mechanism of concentration quenching can be explained by the dipole–dipole interaction. Through the theoretical calculation, the color purity of the as-prepared  $\text{Sr}_5(\text{PO}_4)_3\text{Cl}:\text{Eu}^{2+}$  phosphor is much better than the commercial compound, blue emitting  $\text{BaMgAl}_{10}\text{O}_7:\text{Eu}^{2+}$  (BAM: $\text{Eu}^{2+}$ ). Particularly, a near-UV white LED was fabricated by using a InGaN-based near-UV LED chip (395 nm) and a mixture of  $\text{Sr}_5(\text{PO}_4)_3\text{Cl}:\text{Eu}^{2+}$ , green-emitting  $(\text{Ba},\text{Sr})_2\text{SiO}_4:\text{Eu}^{2+}$  and red-emitting  $\text{CaAlSiN}_3$  phosphors. The obtained LED device exhibits an excellent color-rendering index ( $R_a = 94.65$ ) at a correlated color temperature of 3567.84 K with CIE coordinates of (0.3952, 0.3709). The above results suggest that the  $\text{Sr}_5(\text{PO}_4)_3\text{Cl}:\text{Eu}^{2+}$  phosphor is a promising blue-emitting phosphor for the application in near-UV white light-emitting diodes.

## Introduction

In recent years, white light-emitting diodes (w-LEDs) have attracted significant attention owing to their satisfactory advantages of energy saving properties, long lifetime, high efficiency as well as high material stability.<sup>1,2</sup> Because of this, w-LEDs are considered to be a potential candidate for the replacement of conventional incandescent and fluorescent lamps and treated as the next-generation solid-state lighting systems.<sup>3-5</sup> Typically, a commercial w-LED is generated by the combination of a blue InGaN based-LED with a yellow-emitting  $\text{Y}_3\text{Al}_5\text{O}_{12}:\text{Ce}^{3+}$  (YAG: $\text{Ce}^{3+}$ ) phosphor. However, due to the deficiency of sufficient red emission in the visible spectrum, this type of white LEDs has several disadvantages such as a low color-rendering index (CRI) and high correlated color temperature (CCT). Particularly, the white light generated in this way is different from the nature light and thus some primary applications are restricted.<sup>6-8</sup> In order to solve this issue and generate white light with excellent CRI values and suitable CCT for solid-state light systems, another approach of pumping trichromatic (blue, green and red) phosphors with a near-UV light chip (350-420 nm) has been widely investigated.<sup>7,9-11</sup>

Nowadays,  $\text{Eu}^{2+}$  ion is the most frequently used activator in the phosphor, and its emission and absorption spectra usually consist of a broad band due to transitions from the  $4f^7$  ground state to the  $4f^65d$  excited state.<sup>6</sup> Furthermore,  $\text{Eu}^{2+}$  ion can emit light from the UV to the infrared with broad band emitting luminescence on different host matrices since the involved 5d orbital of  $\text{Eu}^{2+}$  ion is external and strongly influenced by

the crystal field.<sup>12</sup> Due to these excellent properties,  $\text{Eu}^{2+}$  ion-doped phosphors have been widely studied in LED applications.<sup>13-16</sup> Previous works show that  $\text{Eu}^{2+}$  ion-activated phosphates have low synthesis temperature, high thermal stability and high luminescence efficiency.<sup>17-19</sup> For example,  $\text{KMg}_4(\text{PO}_4)_3:\text{Eu}^{2+}$ ,<sup>6</sup>  $\text{Li}_3\text{Sc}(\text{PO}_4)_3:\text{Eu}^{2+}$ ,<sup>15</sup>  $\text{Sr}_8\text{MgGd}(\text{PO}_4)_7:\text{Eu}^{2+}$ ,<sup>20</sup> have been demonstrated as useful luminescent materials for the fabrication of high-performance LED devices.

In 1974, Wu and co-workers firstly reported the crystal structure of  $\text{Sr}_5(\text{PO}_4)_3\text{Cl}$  phosphate.<sup>21</sup> Subsequently, Dhoble firstly reported the luminescence properties of  $\text{Sr}_5(\text{PO}_4)_3\text{Cl}:\text{Eu}^{2+}$  phosphor in 2000.<sup>22</sup> Afterwards, Kang et al. reported the improved luminescence of  $\text{Sr}_5(\text{PO}_4)_3\text{Cl}:\text{Eu}^{2+}$  phosphor prepared by flame spray method in 2003.<sup>23</sup> In 2014, Kang et al. reported the luminescence properties of  $\text{Sr}_5(\text{PO}_4)_3\text{Cl}:\text{Eu}^{2+}$  nanobundles using a facile and mild hydrothermal process.<sup>24</sup> However, to the best of our knowledge, there is no report dedicated to the electronic structure, decay lifetime and temperature-dependent luminescence characteristics of  $\text{Sr}_5(\text{PO}_4)_3\text{Cl}:\text{Eu}^{2+}$  phosphor as well as the fabrication of  $\text{Sr}_5(\text{PO}_4)_3\text{Cl}:\text{Eu}^{2+}$  pumped near-UV LED devices. In this work, the crystal structure, electronic structure, reflectance spectra, thermal stability and quantum efficiency of blue-emitting  $\text{Sr}_5(\text{PO}_4)_3\text{Cl}:\text{Eu}^{2+}$  phosphor, as well as its application in near-UV white light-emitting diodes have been investigated systematically. The white LEDs were fabricated by using a InGaN-based near-UV LED chip (395 nm) and a mixture of  $\text{Sr}_5(\text{PO}_4)_3\text{Cl}:\text{Eu}^{2+}$ , green-emitting  $(\text{Ba},\text{Sr})_2\text{SiO}_4:\text{Eu}^{2+}$  and

red-emitting CaAlSiN<sub>3</sub> phosphors, and the optical properties of LED devices were also studied. The results suggest that the Sr<sub>5</sub>(PO<sub>4</sub>)<sub>3</sub>Cl:Eu<sup>2+</sup> phosphor is a suitable blue-emitting candidate for the application in near-UV white light emitting diodes.

## 2. Materials and Method

### 2.1 Synthesis of Sr<sub>5-x</sub>(PO<sub>4</sub>)<sub>3</sub>Cl:xEu<sup>2+</sup>

A series of samples with a general formula of Sr<sub>5-x</sub>(PO<sub>4</sub>)<sub>3</sub>Cl:xEu<sup>2+</sup> ( $x = 0, 0.005, 0.01, 0.02, 0.03, 0.05$  and  $0.07$ ; i.e. 0 at. %, 0.5 at. %, 1 at. %, 2 at. %, 3 at. %, 5 at. % and 7 at. %) was prepared by solid state reactions as follows. NH<sub>4</sub>H<sub>2</sub>PO<sub>4</sub> (AR), SrCO<sub>3</sub> (AR), NH<sub>4</sub>Cl (AR) and Eu<sub>2</sub>O<sub>3</sub> (4N) were used as starting materials. These materials were weighed according to the stoichiometric ratio of the formula and ground together in an agate mortar. Thereafter, the mixtures were transferred to corundum crucibles accordingly and then these corundum crucibles were placed in a big high-purity graphite crucible. The high-purity graphite crucible was put into a muffle furnace and precalcined at 400 °C for 1 h, and subsequently further sintered at 1050 °C for 5 h. Finally, the furnace cooled down to room temperature naturally and the mixtures were ground in an agate mortar.

### 2.2 Characterization

The crystalline phase of the synthesized Sr<sub>5</sub>(PO<sub>4</sub>)<sub>3</sub>Cl:Eu<sup>2+</sup> was verified by X-ray diffraction (XRD) patterns using Panalytical X-Pert PRO diffractometer with a Cu K $\alpha$  (40.0 KV, 30.0 mA) radiation ( $\lambda=1.5418$  Å). Photoluminescence excitation (PLE) and emission (PL) spectra were measured by Hitachi F-7000 spectrofluorometer equipped

with a 150 W Xenon lamp as an excitation source. The diffuse reflectance spectra were measured by Cary 5000 UV-VIS-NIR spectrophotometer. The photoluminescence decays were recorded by using a standard Edinburgh Instruments FLS920 spectrometer with Tsuna-mi plus GWU system pumped by YAG:Nd laser. The internal QEs of these samples were measured using a standard Edinburgh Instruments FLS980 spectrometer equipped with an integrating sphere attachment. The measured samples were placed in the integrating sphere and the Xe lamp was employed as the light source to pump the samples. The QE was obtained by comparing the spectral intensity of the light source and the emission intensity of the sample. The meter of Keithley 2611 was used to supply a current of 350 mA for illumination of the fabricated LEDs and the electroluminescent spectra of the fabricated LEDs were measured by using the SP320 spectrometer with an integrating sphere manufactured by Instrument Systems Inc. All the above-mentioned measurements were conducted at room temperature. The temperature-dependent PL spectra within the temperature range of 300–500 K were measured by Edinburgh Instruments FSP920 spectrometer.

### 2.3 Computational details

All the calculations of the  $\text{Sr}_5(\text{PO}_4)_3\text{Cl}$  host matrix was performed using the projector-augmented wave (PAW) method within the density functional theory (DFT), as implemented in the Vienna ab initio simulation package (VASP)<sup>25-28</sup> Exchange and correlation functional was treated within generalized gradient approximation (GGA) of the Perdew-Burke-Ernzerhof (PBE) formula.<sup>29</sup> Wave functions were expanded in plane

waves up to a kinetic energy cutoff of 520 eV. The lattice vectors (both unit cell shape and size) are fully relaxed together with atomic coordinates until the Hellmann-Feynman force on each atom less than 0.01 eV/Å. Brillouin-zone integrations were approximated by using special k-point sampling of Monkhorst-Pack scheme with a  $7 \times 7 \times 7$  mesh.

### 3. Results and discussion

#### 3.1 Optimization of lattice parameters and electronic structure of $\text{Sr}_5(\text{PO}_4)_3\text{Cl}$ host

The optimization of the geometry of the  $\text{Sr}_5(\text{PO}_4)_3\text{Cl}$  host matrix was investigated using the DFT calculations. The calculated results were summarized in Table 1. The results indicated that the calculated lattice parameters and cell volume of  $\text{Sr}_5(\text{PO}_4)_3\text{Cl}$  agree well with the experimental results reported by Wu and co-workers<sup>24</sup> (the differences between experimental and theoretical values for  $a$ ,  $c$  and  $V$  are within 1.38%, 0.94% and 3.57%, respectively).

In general, if a host matrix has a band gap more than 3eV, it will be an appropriate candidate for luminescence materials since this high band gap is able to accommodate both the ground and excited states of luminescent ion centers.<sup>3</sup> The band structure of  $\text{Sr}_5(\text{PO}_4)_3\text{Cl}$  along high symmetry points of the Brillouin zone of the hexagonal crystal is shown in Fig. 1.<sup>30</sup> One can see that  $\text{Sr}_5(\text{PO}_4)_3\text{Cl}$  has a wide indirect band gap of approximately 5.01 eV from the top of valence band at M point to the bottom of

conduction band at  $\Gamma$  point. From the calculation results, we can infer that  $\text{Sr}_5(\text{PO}_4)_3\text{Cl}$  is a suitable host matrix to accommodate  $\text{Eu}^{2+}$  ions as emitting centers.

To further understand the detailed composition of the energy bands, the density of states of  $\text{Sr}_5(\text{PO}_4)_3\text{Cl}$  was calculated. Fig. 2 shows the calculated total density of states of  $\text{Sr}_5(\text{PO}_4)_3\text{Cl}$  and projected density of states for Sr, P, O and Cl atoms. It is clearly observed that the conduction band is mainly composed of Sr-4*d*, P-2*p*, O-2*p* and Cl-3*p* states ranging from 4.1 to 8 eV (the bottom of conduction band is dominated by Sr-4*d* state) and that the valence band is mainly composed of O-2*p* and Sr-3*p* below the Fermi level (the top of valence band is dominated by O-2*p* state). The results suggest that the host absorption at near-UV region for the  $\text{Sr}_5(\text{PO}_4)_3\text{Cl}$  host is dominated by the charge transitions from the O-2*p* to Sr-4*d* states.

### 3.2 Crystal structure and morphology characteristics of the $\text{Sr}_5(\text{PO}_4)_3\text{Cl}:\text{Eu}^{2+}$ phosphors

Fig. 3 depicts the XRD patterns of  $\text{Sr}_{5-x}(\text{PO}_4)_3\text{Cl}:x\text{Eu}^{2+}$  ( $x = 0, 0.005, 0.01, 0.02, 0.03, 0.05$  and  $0.07$ ) samples (the standard data card ICSD#174336 of  $\text{Sr}_5(\text{PO}_4)_3\text{Cl}$  is provided as a reference). It can be found that all the XRD patterns agree well with the standard data card and that introducing of  $\text{Eu}^{2+}$  has not brought about obvious change in the  $\text{Sr}_5(\text{PO}_4)_3\text{Cl}$  host structure. Fig. 4 (a) shows the crystal structure of  $\text{Sr}_5(\text{PO}_4)_3\text{Cl}$  viewed along the *c*-axis. It can be found that  $\text{Sr}_5(\text{PO}_4)_3\text{Cl}$  has a phase of hexagonal structure with a space group of P 63/m (176). Fig. 4 (b) presents the coordination

environment of  $\text{Sr}^{2+}$  ions, indicating that  $\text{Sr}^{2+}$  ions in  $\text{Sr}_5(\text{PO}_4)_3\text{Cl}$  have two ways of coordination (one is six-fold coordinated by  $\text{O}^{2-}$  ions and the other is surrounded by five  $\text{O}^{2-}$  and two  $\text{Cl}^-$  ions). In this case, we believe that  $\text{Eu}^{2+}$  ions ( $r = 1.17 \text{ \AA}$  for CN = 6 and 1.20 for CN = 7) will randomly substitute  $\text{Sr}^{2+}$  ( $r = 1.18 \text{ \AA}$  for CN = 6 and  $r = 1.21 \text{ \AA}$  for CN = 7) sites.

### 3.3 Luminescence properties of $\text{Sr}_5(\text{PO}_4)_3\text{Cl}:\text{Eu}^{2+}$ phosphors

Fig. 5(a) shows the diffuse reflectance spectra (DRS) of pure  $\text{Sr}_5(\text{PO}_4)_3\text{Cl}$  host matrix and a typical  $\text{Sr}_{4.99}(\text{PO}_4)_3\text{Cl}:0.01\text{Eu}^{2+}$  sample. It can be found that the  $\text{Sr}_5(\text{PO}_4)_3\text{Cl}$  has a broad absorption from 190 to 400 nm and a high reflection ranging from 400 to 700 nm. The band gap of  $\text{Sr}_5(\text{PO}_4)_3\text{Cl}$  host can be obtained from the following equation:<sup>6, 31</sup>

$$[F(R_\infty)hv]^n = C (hv - E_g) \quad (1)$$

where  $F(R_\infty)$  is the Kubelka-Munk function ( $R_\infty$  is equal to  $R_{\text{sample}}/R_{\text{standard}}$ ),  $hv$  is the energy per photon,  $C$  is a constant,  $E_g$  is the value of the band gap, and  $n$  is a transition coefficient (for an indirect allowed transition,  $n$  equals to 0.5; for a direct allowed transition,  $n$  equals to 2; for a direct forbidden transition,  $n$  equals to 3).  $F(R_\infty)$  can be formulated to the following equation:<sup>32</sup>

$$F(R_\infty) = \frac{K}{S} = \frac{(1-R)^2}{R} \quad (2)$$

where  $K$ ,  $S$  and  $R$  are the absorption, scattering and reflectance parameters, respectively. As mentioned before, the  $\text{Sr}_5(\text{PO}_4)_3\text{Cl}$  is calculated to be an indirect band gap material

by using DFT, so we set the  $n$  value as 0.5. As shown in Fig. 5(b), the band gap energy of  $\text{Sr}_5(\text{PO}_4)_3\text{Cl}$  host is estimated to be about 5.03 eV from the extrapolation of the linear line for  $[F(R_\infty)h\nu]^n = 0$ . The result is consistent with DFT calculation of a band gap of 5.01 eV. The DRS of the  $\text{Sr}_{4.99}(\text{PO}_4)_3\text{Cl}:0.01\text{Eu}^{2+}$  sample shows strong broad absorption ranging from 190 to 440 nm, which fits well with the excitation spectrum, indicating that  $\text{Eu}^{2+}$  ions were well introduced to the  $\text{Sr}_5(\text{PO}_4)_3\text{Cl}$  host.

The PL excitation ( $\lambda_{\text{em}} = 444$  nm) and PL emission ( $\lambda_{\text{ex}} = 245, 277, 341, 365, 385$  and 405 nm) spectra of the  $\text{Sr}_{4.99}(\text{PO}_4)_3\text{Cl}:0.01\text{Eu}^{2+}$  phosphor are also shown in Fig. 5(a). The PLE spectrum shows a broad emission band from 240 to 420 nm, which originates from the transition from  $4f^7$  ( $^8\text{S}_{7/2}$ ) ground to  $4f^65d^1$ -excited level of  $\text{Eu}^{2+}$  ion.<sup>33</sup> The PL spectra of the  $\text{Sr}_{4.99}(\text{PO}_4)_3\text{Cl}:0.01\text{Eu}^{2+}$  phosphor under various excitation wavelengths present the similar profile with a broad blue emission band ranging from 410 to 490 nm peaking at 444 nm, which is attributed to the lowest relaxed  $4f^65d^1$  level to the  $4f^7$  ( $^8\text{S}_{7/2}$ ) level of  $\text{Eu}^{2+}$  ions. As we know, the emission position of  $\text{Eu}^{2+}$  ions is highly related to its local environment. In the  $\text{Sr}_5(\text{PO}_4)_3\text{Cl}$  host, there are two sites for  $\text{Eu}^{2+}$  ions to occupy. Thus, deconvolution of PL emission spectra was used to identify two emission bands correlated with the occupation of  $\text{Eu}^{2+}$  ions. Fig. 6 shows the deconvoluted PL emission spectra of the  $\text{Sr}_{4.99}(\text{PO}_4)_3\text{Cl}:0.01\text{Eu}^{2+}$  phosphor using two Gaussian equations with reasonable fitting values. One can see that two peaks are present in the deconvolution of the emission band: one is located at ~442 nm and the other is located

at ~455 nm. In general, any small change in the crystal disorder or lack of charge neutrality will influence the local environment of  $\text{Eu}^{2+}$  ions, so it is different to assign an emission band to a particular crystallographic site.<sup>33</sup> However, we can use the famous empirical theory by Van Uitert to infer it. According to the Van Uitert theory, the position of the d-band edge in energy for rare earth ions ( $E$ ) ( $\text{cm}^{-1}$ ) can be calculated using the following equation:<sup>16,34</sup>

$$E = Q \left[ 1 - \left( \frac{V}{4} \right)^{1/V} \times 10^{-(n \cdot E_a \cdot r)/80} \right] \quad (3)$$

where  $Q$  stands for the position in energy for the lower d-band edge for the free  $\text{Eu}^{2+}$  ions ( $\text{cm}^{-1}$ ),  $n$  is the number of anions in the immediate shell around the  $\text{Eu}^{2+}$  ion,  $V$  is the valence of the  $\text{Eu}^{2+}$  ion,  $E_a$  is the electron affinity of anion atom (in eV), and  $r$  is the radius of the host cation replaced by the  $\text{Eu}^{2+}$  ion (in Å). By substituting specific coordination numbers into the empirical formula with the corresponding  $n$ ,  $E_a$  and  $r$  values, we can infer that the  $\text{Sr}^{2+}$  ions with seven coordination numbers can be assigned to the deconvoluted Gaussian curve peaking at 442 nm ( $22624 \text{ cm}^{-1}$ ), while the  $\text{Sr}^{2+}$  ions with six coordination numbers can be assigned to the deconvoluted Gaussian curve peaking at 455 nm ( $21978 \text{ cm}^{-1}$ ).

Moreover, the emission chromaticity coordinates for the spectrum under 277 nm light excitation of  $\text{Sr}_{4.99}(\text{PO}_4)_3\text{Cl}:0.01\text{Eu}^{2+}$  have been calculated by using the CIE 1931 color matching functions.<sup>35, 36</sup> Fig. 7 shows the CIE chromaticity diagram of the  $\text{Sr}_{4.99}(\text{PO}_4)_3\text{Cl}:0.01\text{Eu}^{2+}$  phosphor and the commercial blue phosphor  $\text{BaMgAl}_{10}\text{O}_7:\text{Eu}^{2+}$

(BAM:Eu<sup>2+</sup>), respectively. The CIE chromaticity coordinates of Sr<sub>4.99</sub>(PO<sub>4</sub>)<sub>3</sub>Cl:0.01Eu<sup>2+</sup> and BAM:Eu<sup>2+</sup> are determined to be (0.1540, 0.0230) and (0.1417, 0.1072), respectively.<sup>1</sup> Since the color purity of phosphor is an important feature to evaluate phosphor chromaticity property,<sup>37, 38</sup> the color purity of luminescent materials can be calculated using the following equation:<sup>36, 39</sup>

$$\text{Color purity} = \frac{\sqrt{(x-x_i)^2+(y-y_i)^2}}{\sqrt{(x_d-x_i)^2+(y_d-y_i)^2}} \cdot 100\% \quad (5)$$

where  $(x, y)$  is the color coordinate of the light source,  $(x_i, y_i)$  is the CIE of equal-energy illuminant with a value of (0.3333, 0.3333), and  $(x_d, y_d)$  is the chromaticity coordinate corresponding to the dominant wavelength of the light source. The CIE coordinates  $(x, y)$  of Sr<sub>4.99</sub>(PO<sub>4</sub>)<sub>3</sub>Cl:0.01Eu<sup>2+</sup> and BAM:Eu<sup>2+</sup> are (0.1540, 0.0230) and (0.1417, 0.1072), respectively. The dominant wavelength points of Sr<sub>4.99</sub>(PO<sub>4</sub>)<sub>3</sub>Cl:0.01Eu<sup>2+</sup> and BAM:Eu<sup>2+</sup> are determined to be 453.4 and 473.3 nm, respectively, and we can obtain that the  $(x_d, y_d)$  chromaticity coordinates for Sr<sub>4.99</sub>(PO<sub>4</sub>)<sub>3</sub>Cl:0.01Eu<sup>2+</sup> and BAM:Eu<sup>2+</sup> are (0.2075, 0.0465) and (0.1416, 0.14607), respectively. By substituting the coordinates of  $(x, y)$ ,  $(x_i, y_i)$ ,  $(x_d, y_d)$  to Eq. (5), the color purities of Sr<sub>4.99</sub>(PO<sub>4</sub>)<sub>3</sub>Cl:0.01Eu<sup>2+</sup> and BAM:Eu<sup>2+</sup> are determined to be 99.0% and 88.0%, respectively. This result indicates that Sr<sub>5</sub>(PO<sub>4</sub>)<sub>3</sub>Cl : Eu<sup>2+</sup> phosphor is a deep blue phosphor and features a higher color purity compared with commercial blue phosphor BAM:Eu<sup>2+</sup>. The inset of Fig. 7 shows the digital image excited at 365 nm in the UV lamp for the Sr<sub>4.99</sub>(PO<sub>4</sub>)<sub>3</sub>Cl:0.01Eu<sup>2+</sup>

phosphor, which indicates that  $\text{Sr}_5(\text{PO}_4)_3\text{Cl}:\text{Eu}^{2+}$  is a suitable candidate as a blue-emitting phosphor for the application in w-LEDs.

The PLE ( $\lambda_{\text{em}} = 444 \text{ nm}$ ) and PL ( $\lambda_{\text{ex}} = 277 \text{ nm}$ ) spectra of  $\text{Sr}_{5-x}(\text{PO}_4)_3\text{Cl}:x\text{Eu}^{2+}$  ( $x = 0.005, 0.01, 0.02, 0.03, 0.05$  and  $0.07$ ) as a function of the concentration of  $\text{Eu}^{2+}$  ions are shown in Fig. 8 (a) and (b). One can see that all the PLE and PL spectra of  $\text{Sr}_{5-x}(\text{PO}_4)_3\text{Cl}:x\text{Eu}^{2+}$  samples are similar. The excitation and emission intensity initially increases with the increase of the content of  $\text{Eu}^{2+}$  ions until a maximum intensity is reached when  $x = 0.01$ , and then it decreases with a further increase of the content of  $\text{Eu}^{2+}$  ions due to concentration quenching of  $\text{Eu}^{2+}$  ions.<sup>40</sup> The occurrence of concentration quenching at a higher  $\text{Eu}^{2+}$  content is caused by the energy consumed via energy transfer from one activator to another.<sup>17</sup> The concentration quenching process is dependent on the critical transfer distance ( $R_c$ ), which is the shortest average distance between the nearest activator  $\text{Eu}^{2+}$  ions at a critical concentration  $x_c$ . Hence, it is necessary to obtain the critical transfer distance ( $R_c$ ) for further understanding the mechanism of concentration quenching. Blasse pointed out that, if  $V$  is the volume of the unit cell,  $x_c$  is the optimal concentration,  $N$  is the number of cations in the unit cell, the critical transfer distance can be calculated using the following formula:<sup>41</sup>

$$R_c = 2\left(\frac{3V}{4\pi x_c N}\right)^{1/3} \quad (6)$$

For the  $\text{Sr}_5(\text{PO}_4)_3\text{Cl}$  host, the values of  $N$ ,  $V$  and  $x_c$  are 10,  $606.58 \text{ \AA}^3$  and 0.01, respectively. Using Eq.(5),  $R_c$  is obtained to be  $22.63 \text{ \AA}$ . As we know, the typical critical

distance of the exchange interaction is about 5 Å and the exchange interaction only matches the energy transfer of forbidden transitions. Thus, the electric multipolar interactions are dominant in the energy transfer process. According to the Dexter theory, the interaction mechanism can be inferred by the equation as follows:<sup>42</sup>

$$I/x = K[1 + \beta(x)^{Q/3}]^{-1} \quad (7)$$

where K and  $\beta$  are constants for the same excitation condition of a given host crystal;  $x$  is the activator concentration;  $Q = 6, 8,$  and  $10$  is for dipole–dipole (d-d), dipole–quadrupole (d-q), and quadrupole–quadrupole (q-q) interactions, respectively. The curve of  $\lg(I/x)$  versus  $\lg(x)$  is shown in Fig. 9. From Fig. 9, one can see that the plot is linear and that the slope of the fitted straight line equals to  $-1.6692$ . The value of  $Q$  deduced from Eq. (6) is  $5.0076$ , which is approximately equal to  $6$ . This result indicates that the major mechanism for the concentration quenching of the  $\text{Sr}_5(\text{PO}_4)_3\text{Cl}:\text{Eu}^{2+}$  phosphor is the dipole–dipole interaction.

In order to further confirm the concentration quenching effect of  $\text{Sr}_{5-x}(\text{PO}_4)_3\text{Cl}:x\text{Eu}^{2+}$  phosphors, room-temperature photoluminescence decay curves for the  $\text{Sr}_{5-x}(\text{PO}_4)_3\text{Cl}:x\text{Eu}^{2+}$  ( $x = 0.005, 0.01, 0.02, 0.03$  and  $0.05$ ;  $\lambda_{\text{ex}} = 277$  nm,  $\lambda_{\text{em}} = 444$  nm) phosphors were also investigated. As shown in Fig.10, the decay curves can be fitted to a single-exponential decay model by the following equation:<sup>43</sup>

$$I(t) = I_0 + A_1 \exp(-t/\tau) \quad (8)$$

where  $I$  and  $I_0$  are the luminescence intensities at times  $t$  and 0, respectively,  $A_1$  is a constant and  $\tau$  is the decay time. The lifetimes for  $\text{Sr}_{5-x}(\text{PO}_4)_3\text{Cl}:x\text{Eu}^{2+}$  ( $x = 0.005, 0.01, 0.02, 0.03$  and  $0.05$ ) are calculated to be 492.87, 527.93, 520.38, 501.11 and 469.59 ns, respectively. One can see that the decay time initially increases from 492.87 ns at  $x = 0.005$  to 527.93 ns at  $x = 0.01$ , and then shows a tendency of decrease with a further increase of the content of  $\text{Eu}^{2+}$  ions, reaching a value of 469.59 ns at  $x = 0.05$ . This result confirms that there exists an efficient energy transfer between  $\text{Eu}^{2+}$  ions and this causes concentration quenching with an increased content of  $\text{Eu}^{2+}$  ions. Moreover, we can find that all the measured decay times are reasonable for the  $5d-4f$  transition of  $\text{Eu}^{2+}$  in solids ( $\sim 1\mu\text{s}$ ).<sup>6</sup>

### 3.4 Thermal quenching properties of $\text{Sr}_5(\text{PO}_4)_3\text{Cl}:\text{Eu}^{2+}$ phosphors.

The thermal stability of the phosphor is an important technological parameter in evaluating its potential for the LED application due to its influence on the light output, service life and color rendering index.<sup>4,44</sup> Since the most used commercial InGaN-based near-UV LED chip is 395 nm emitting chip due to its low price and high efficiency,<sup>33</sup> we used a 395 nm InGaN-based near-UV LED chip to fabricate w-LED device in this work. The temperature-dependent emission spectra of the  $\text{Sr}_{4.99}(\text{PO}_4)_3\text{Cl}:0.01\text{Eu}^{2+}$  phosphor measured at 300 to 500 K under 395 nm light excitation were shown in Fig. 11. It can be found that the intensity of emission gradually decreases from 100% to 77.68% (taking the intensity of emission measured at 300 K as a unity) when the

measured temperature increases from 300 to 500 K. The inset of Fig. 11 shows the comparison of the thermal luminescence quenching of  $\text{Sr}_{4.99}(\text{PO}_4)_3\text{Cl}:0.01\text{Eu}^{2+}$  phosphor and commercial blue  $\text{BAM}:\text{Eu}^{2+}$  phosphor. It can be found that the emission intensity measured at 423 K (150 °C) drops to 87.61% of the initial value measured at 300 K, while the emission intensity of the commercial  $\text{BAM}:\text{Eu}^{2+}$  phosphor decreases to 88.31% of the initial value measured at 300 K. The result indicates that  $\text{Sr}_5(\text{PO}_4)_3\text{Cl}:\text{Eu}^{2+}$  almost features the same thermal stability as commercial blue  $\text{BAM}:\text{Eu}^{2+}$  phosphor, confirming the good stability of this phosphor and the potential application in the high-power LEDs.

To further investigate temperature-dependent thermal quenching phenomenon, the activation energy for the thermal quenching has been estimated via using the Arrhenius equation:<sup>45,46</sup>

$$I(T) = \frac{I_0}{1 + c \exp\left(-\frac{\Delta E}{kT}\right)} \quad (9)$$

where  $c$  is a constant,  $k$  is the Boltzmann's constant with a value of  $8.62 \times 10^{-5}$  eV/K,  $I_0$  is the initial emission intensity measured at room temperature,  $I(T)$  is the emission intensity measured at different temperatures, and  $\Delta E$  is the activation energy for the thermal quenching. The plot of  $\ln[(I_0/I)-1]$  versus  $1/(kT)$  is shown in Fig. 12, and a straight line is used to fit this curve up to 500 K. The activation energy  $\Delta E$  for the thermal quenching is obtained to be 0.194 eV using Eq. (9). The high activation energy

achieved in this work indicates that this phosphor features a good thermal stability and is an excellent candidate for the application in high-power LEDs.

### 3.5 Quantum efficiency and electroluminescent properties of fabricated white

#### LEDs

Quantum efficiency of phosphors is another important factor in evaluating its potential for the LED application.<sup>47</sup> The  $\text{Sr}_{4.99}(\text{PO}_4)_3\text{Cl}:0.01\text{Eu}^{2+}$  phosphor was investigated by the absolute quantum efficiencies. The measured internal QE of the  $\text{Sr}_{4.99}(\text{PO}_4)_3\text{Cl}:0.01\text{Eu}^{2+}$  phosphor was estimated to be 80.53 % under the 395 nm excitation. This relatively high internal QE obtained by 395 nm excitation confirms that the  $\text{Sr}_5(\text{PO}_4)_3\text{Cl}:\text{Eu}^{2+}$  phosphor is suitable for the application in 395 nm InGaN-based near-UV LED chip. Table 3 concludes excitation wavelength, emission peak, and internal QE of  $\text{Sr}_5(\text{PO}_4)_3\text{Cl}:\text{Eu}^{2+}$ , some latest reported  $\text{Eu}^{2+}$  doped blue-emitting phosphors and commercial blue phosphor  $\text{BAM}:\text{Eu}^{2+}$ .<sup>6, 33, 48</sup> It can be found that the internal QE achieved in our work is superior to some latest reported  $\text{Eu}^{2+}$  blue phosphors. However, the internal QE is relatively lower compared with the commercial blue phosphor  $\text{BAM}:\text{Eu}^{2+}$  with an internal QE of 88.99%.<sup>6</sup> Hence, the luminescence performance of the  $\text{Sr}_5(\text{PO}_4)_3\text{Cl}:\text{Eu}^{2+}$  phosphor can be improved in future work since the QE of phosphors highly depends on the preparation conditions, crystalline defects, particle size and morphology.<sup>49</sup>

To substantiate the potential application of the  $\text{Sr}_5(\text{PO}_4)_3\text{Cl}:\text{Eu}^{2+}$  phosphor, a near-UV white LED was fabricated by using a InGaN-based near-UV LED chip (395 nm) and a mixture of  $\text{Sr}_5(\text{PO}_4)_3\text{Cl}:\text{Eu}^{2+}$ , green-emitting  $(\text{Ba,Sr})_2\text{SiO}_4:\text{Eu}^{2+}$  and red-emitting  $\text{CaAlSiN}_3$  phosphors. The electroluminescent spectrum of the fabricated w-LED, which was driven using a current of 350 mA and a voltage of 3.29 V, is shown in Fig. 13. The CCT,  $R_a$ , and CIE color coordinates of this fabricated w-LED are detected to be 3567.84 K, 94.65 and (0.3952, 0.3790), respectively. The  $R_a$  of the fabricated w-LED was obtained from the full set of the 14 CRIs and is shown in Table 2. These warm CCT value (3567.84 K) and high  $R_a$  (94.65) indicate that  $\text{Sr}_5(\text{PO}_4)_3\text{Cl}:\text{Eu}^{2+}$  is a potential candidate as a green phosphor for the application in the near-UV warm white light emitting diodes.

#### 4. Conclusions

In conclusion, a series of  $\text{Eu}^{2+}$  doped  $\text{Sr}_5(\text{PO}_4)_3\text{Cl}$  blue-emitting phosphors was synthesized by conventional high-temperature solid-state reactions. The lattice parameters and the electronic structure of the  $\text{Sr}_5(\text{PO}_4)_3\text{Cl}$  host matrix were investigated using DFT calculations. The calculated results show that the band gap of  $\text{Sr}_5(\text{PO}_4)_3\text{Cl}$  host matrix matches well with the experiment and that  $\text{Sr}_5(\text{PO}_4)_3\text{Cl}$  is a suitable host matrix to accommodate  $\text{Eu}^{2+}$  ions as emitting centers. The concentration quenching of  $\text{Eu}^{2+}$  ions in the  $\text{Sr}_5(\text{PO}_4)_3\text{Cl}$  host is determined to be 1.0 mol% and the mechanism of concentration quenching can be explained by the dipole–dipole interaction. The color

purity of the as-prepared  $\text{Sr}_5(\text{PO}_4)_3\text{Cl}:\text{Eu}^{2+}$  phosphor is determined to be 99.0 %, which is higher than that of the commercial blue emitting  $\text{BAM}:\text{Eu}^{2+}$ . The measured temperature-dependent emission spectra suggest that the  $\text{Sr}_5(\text{PO}_4)_3\text{Cl}:\text{Eu}^{2+}$  phosphor has an excellent thermal stability. Moreover, the obtained LED device exhibits an excellent color-rendering index ( $R_a = 94.65$ ) at a correlated color temperature of 3567.84 K with CIE coordinates of (0.3952, 0.3709). Our results display that the  $\text{Sr}_5(\text{PO}_4)_3\text{Cl}:\text{Eu}^{2+}$  phosphor is an excellent candidate as a blue-emitting phosphor for the application in near-UV w-LEDs.

### Acknowledgments

This work was supported by the National Natural Science Foundation of China (Grant No. 61076056), Fujian Provincial Department of Science & Technology (Grant No. 2015H0036), the Fundamental Research Funds for the Central Universities (Grant No. 2013SH004), Program for New Century Excellent Talents in Fujian Province University (NCETFJ), Scientific Research Foundation for the Returned Overseas Chinese Scholars, State Education Ministry, China. We thank Dr. Jian Chen (China University of Geosciences (Beijing), China) for measurement of temperature-dependent emission spectra, thank Dr. YongJie Wang (Chongqing University of Posts and Telecommunications, China) for measurement of luminescence decay curves.

## References

1. W. R. Liu, C. H. Huang, C. P. Wu, Y. C. Chiu, Y. T. Yeh and T. M. Chen, *J. Mater. Chem.*, 2011, **21**, 6869.
2. X. Li, J. D. Budai, F. Liu, J. Y. Howe, J. Zhang, X.-J. Wang, Z. Gu, C. Sun, R. S. Meltzer and Z. Pan, *Light: Sci. Appl.*, 2013, **2**, e50.
3. N. Zhang, C. Guo, J. Zheng, X. Su and J. Zhao, *J. Mater. Chem. C*, 2014, **2**, 3988.
4. K. Li, J. Xu, X. Cai, J. Fan, Y. Zhang, M. Shang, H. Lian and J. Lin, *J. Mater. Chem. C*, 2015, DOI: 10.1039/c5tc00796h.
5. Y. Li, J. Wang, W. Zhou, G. Zhang, Y. Chen and Q. Su, *Appl. Phys. Express*, 2013, **6**, 082301.
6. J. Chen, Y. Liu, L. Mei, H. Liu, M. Fang and Z. Huang, *Sci. Rep.*, 2015, **5**, 9673.
7. Z. Xia, Y. Zhang, M. S. Molokeev and V. V. Atuchin, *J. Phys. Chem. C*, 2013, **117**, 20847-20854.
8. J. Zhou, Z. Xia, M. Yang and K. Shen, *J. Mater. Chem.*, 2012, **22**, 21935.
9. S. P. Lee, T. S. Chan and T. M. Chen, *ACS Appl. Mater. Inter.*, 2015, **7**, 40-44.
10. M. Shang, C. Li and J. Lin, *Chem. Soc. Rev.*, 2014, **43**, 1372-1386.
11. M. Jiao, Y. Jia, W. Lü, W. Lv, Q. Zhao, B. Shao and H. You, *J. Mater. Chem. C*, 2014, **2**, 4304.
12. X. Lan, Q. Wei, Y. Chen and W. Tang, *Opt. Mater.*, 2012, **34**, 1330-1332.

13. P. Pust, V. Weiler, C. Hecht, A. Tucks, A. S. Wochnik, A. K. Henss, D. Wiechert, C. Scheu, P. J. Schmidt and W. Schnick, *Nat. Mater.*, 2014, **13**, 891-896.
14. Z. C. Wu, H. H. Fu, J. Liu, S. P. Kuang, M.-M. Wu, J. G. Xu and X. J. Kuang, *RSC Adv.*, 2015, DOI: 10.1039/c5ra01755f.
15. S. Yu, Z. Xia, M. S. Molokeev, H. Miao and V. V. Atuchin, *ECS J. Solid. State. Sc.*, 2014, **3**, R159-R163.
16. J. Zheng, L. Ying, Q. Cheng, Z. Guo, L. Cai, Y. Lu and C. Chen, *Mater. Res. Bull.*, 2015, **64**, 51-54.
17. J. Chen, Y. G. Liu, L. Mei, Z. Wang, M. Fang and Z. Huang, *J. Mater. Chem. C*, 2015, **3**, 5516-5523.
18. N. Guo, H. You, Y. Song, M. Yang, K. Liu, Y. Zheng, Y. Huang and H. Zhang, *J. Mater. Chem.*, 2010, **20**, 9061.
19. R. Mi, C. Zhao, Z. Xia and J. McKittrick, *J. Am. Ceram. Soc.*, 2014, **97**, 1802-1808.
20. C. H. Huang, D. Y. Wang, Y. C. Chiu, Y. T. Yeh and T. M. Chen, *RSC Adv.*, 2012, **2**, 9130.
21. K. Sudarsanan, R. A. Young, K. Sudarsanan and R. A. Young, *Acta Cryst.*, 1974, **30**, 1381-1386.
22. S. J. Dhoble, *J. Phys. D Appl. Phys.*, 2000, **33**, 158-161.
23. L. Li, R. Yang, Z. Du, K. Zou, X. Zhang, *Chinese Sci. Bull.*, 2003, **48**, 1558-1560.

24. H. Zou, M. Yan, G. Wang, B. Yuan, J. Huang, F. Gao, Y. Sheng, K. Zheng and Y. Song, *Powder Technol.*, 2014, **254**, 579–582.
25. G. Kresse and J. Hafner, *Phys. Rev. B*, 1997, **55**, 7539.
26. G. Kresse and D. Joubert, *Phys. Rev. B*, 1999, **59**, 1758.
27. G. Kresse and J. Furthmüller, *Phys. Rev. B*, 1996, **54**, 11169.
28. G. Kresse and J. Furthmüller, *Comp. Mater. Sci.*, 1996, **6**, 15-50.
29. J. P. Perdew, K. Burke and M. Ernzerhof, *Phys. Rev. Lett.*, 1996, **77**, 3865.
30. W. Setyawan and S. Curtarolo, *Comp. Mater. Sci.*, 2010, **49**, 299-312.
31. Z. Jiang, Y. Wang and L. Wang, *J. Electrochem. Soc.*, 2009, 157.
32. J. A. F. Fernandez and J. M. F. Rodriguez, *Color Research & Applications*, 2005, **30**, 448-456.
33. S. J. Gwak, P. Arunkumar and W. B. Im, *J. Phys. Chem. C*, 2014, **118**, 2686-2692.
34. L. Van Uitert, *J. Lumin.*, 1984, **29**, 1-9.
35. J. Zheng, Q. Cheng, W. Chen, Z. Guo and C. Chen, *ECS J. Solid. State. Sc.*, 2015, **4**, R72-R77.
36. E. F. Schubert, *Light emitting diodes (second edition)* Cambridge University Press, 2006.
37. Y. C. Li, Y. H. Chang, Y. F. Lin, Y. J. Lin and Y. S. Chang, *Appl. Phys. Lett.*, 2006, **89**, 081110.

38. J. Zheng, J. Feng, Q. Cheng, Z. Guo, L. Cai and C. Chen, *Funct. Mater. Lett.*, 2015, **8**, 1550042.
39. P. Du and J. S. Yu, *Mater. Res. Bull.*, 2015, **70**, 553-558.
40. W. Xiao, X. Zhang, Z. Hao, G. H. Pan, Y. Luo, L. Zhang and J. Zhang, *Inorg. Chem.*, 2015, DOI: 10.1021/ic502773t.
41. G. Blasse, *Phys. Lett. A*, 1968, **28**, 444-445.
42. G. Blasse, *J. Solid State Chem.*, 1986, **62**, 207-211.
43. C. Liu, Z. Xia, Z. Lian, J. Zhou and Q. Yan, *J. Mater. Chem. C*, 2013, **1**, 7139-7147.
44. Y. Li, J. Wang, Y. Huang and H. J. Seo, *J. Am. Ceram. Soc.*, 2010, **93**, 722-726.
45. Y. Li, N. Hirosaki, R. Xie, T. Takeka and M. Mitomo, *J. Solid State Chem.*, 2009, **182**, 301-311.
46. R.-J. Xie, N. Hirosaki, N. Kimura, K. Sakuma and M. Mitomo, *Appl. Phys. Lett.*, 2007, **90**, 19110-191103.
47. S. Miao, Z. Xia, M. S. Molokeev, M. Chen, J. Zhang and Q. Liu, *J. Mater. Chem. C*, 2015, DOI: 10.1039/c5tc00339c.
48. H. J. Song, D. K. Yim, H.-S. Roh, I. S. Cho, S.-J. Kim, Y.-H. Jin, H.-W. Shim, D.-W. Kim and K. S. Hong, *J. Mater. Chem. C*, 2013, **1**, 500.
49. D. Dexter and J. H. Schulman, *J. Chem. Phys.*, 1954, **22**, 1063-1070.

**Table Captions:**

**Table 1** Optimized crystal parameters of  $\text{Sr}_5(\text{PO}_4)_3\text{Cl}$  using the DFT calculations

**Table 2** Full set of the 14 CRIs and  $R_a$  of the fabricated w-LED

**Table 3** Excitation wavelength, emission peak, and internal QE of  $\text{Sr}_5(\text{PO}_4)_3\text{Cl}:\text{Eu}^{2+}$ , some latest reported  $\text{Eu}^{2+}$  doped blue-emitting phosphors and commercial blue phosphor BAM: $\text{Eu}^{2+}$ .

**Figure Captions:**

**Figure 1** Calculated band structure of  $\text{Sr}_5(\text{PO}_4)_3\text{Cl}$ . The Fermi level is set at zero energy.

**Figure 2** Total and partial (Sr, P, O, Cl) density of states for  $\text{Sr}_5(\text{PO}_4)_3\text{Cl}$ .

**Figure 3** XRD patterns of as-prepared  $\text{Sr}_{5-x}(\text{PO}_4)_3\text{Cl}:x\text{Eu}^{2+}$  ( $x = 0, 0.005, 0.01, 0.02, 0.03, 0.05$  and  $0.07$ ) phosphors. The standard data card ICSD#174336 of  $\text{Sr}_5(\text{PO}_4)_3\text{Cl}$  is provide as a reference.

**Figure 4** Crystal structure of  $\text{Sr}_5(\text{PO}_4)_3\text{Cl}$ : view of the  $\text{Sr}_5(\text{PO}_4)_3\text{Cl}$  along the c-axis(a); coordination geometry of anions around the  $\text{Sr}^{2+}$  ions(b).

**Figure 5** (a): Excitation and emission spectra of  $\text{Sr}_{4.99}(\text{PO}_4)_3\text{Cl}:0.01\text{Eu}^{2+}$  ( $\lambda_{\text{em}} = 444$  nm for excitation and  $\lambda_{\text{ex}} = 245, 277, 341, 385$  and  $405$  nm for emission); Diffuse reflectance spectra (DRS) of a pure  $\text{Sr}_5(\text{PO}_4)_3\text{Cl}$  host matrix and a typical  $\text{Sr}_{4.99}(\text{PO}_4)_3\text{Cl}:0.01\text{Eu}^{2+}$  sample. (b): Absorption spectrum of  $\text{Sr}_{4.99}(\text{PO}_4)_3\text{Cl}:0.01\text{Eu}^{2+}$  calculated by the Kubelka-Munk equation.

**Figure 6** Deconvoluted PL emission spectra using two Gaussian equations for the  $\text{Sr}_{4.99}(\text{PO}_4)_3\text{Cl}:0.01\text{Eu}^{2+}$  phosphor ( $\lambda_{\text{ex}} = 277$  nm). Inset shows the geometry of anions around the  $\text{Sr}^{2+}$  ions with six and seven coordination numbers.

**Figure 7** CIE chromaticity coordinate diagram of the  $\text{Sr}_{4.99}(\text{PO}_4)_3\text{Cl}:0.01\text{Eu}^{2+}$  phosphor and the commercial blue phosphor  $\text{BaMgAl}_{10}\text{O}_7:\text{Eu}^{2+}$  (BAM:Eu<sup>2+</sup>). The inset shows a digital image excited at 365 nm in the UV lamp of the  $\text{Sr}_{4.99}(\text{PO}_4)_3\text{Cl}:0.01\text{Eu}^{2+}$  phosphor.

**Figure 8** PLE ( $\lambda_{\text{em}} = 444$  nm) (a) and PL ( $\lambda_{\text{ex}} = 277$  nm) (b) spectra of  $\text{Sr}_{5-x}(\text{PO}_4)_3\text{Cl}:x\text{Eu}^{2+}$  ( $x = 0.005, 0.01, 0.02, 0.03, 0.05$  and  $0.07$ ) as a function of the concentration of  $\text{Eu}^{2+}$  ions.

**Figure 9** Plot of  $\lg(I/x)$  versus  $\lg(x)$  in  $\text{Sr}_{5-x}(\text{PO}_4)_3\text{Cl}:x\text{Eu}^{2+}$  phosphors ( $\lambda_{\text{ex}} = 277$  nm).

**Figure 10** Decay curves of the  $\text{Eu}^{2+}$  emission in the  $\text{Sr}_{5-x}(\text{PO}_4)_3\text{Cl}:x\text{Eu}^{2+}$  ( $x = 0.005, 0.01, 0.02, 0.03$  and  $0.05$ ) phosphors detected at 444 nm.

**Figure 11** Emission spectra of  $\text{Sr}_{4.99}(\text{PO}_4)_3\text{Cl}:0.01\text{Eu}^{2+}$  measured at different temperatures ( $\lambda_{\text{ex}}=395$  nm). The inset shows the relative emission intensity as a function of the temperature.

**Figure 12** Arrhenius fitting of the emission intensity and calculated activation energy for the thermal quenching of  $\text{Sr}_{4.99}(\text{PO}_4)_3\text{Cl}:0.01\text{Eu}^{2+}$ .

**Figure 13** Electroluminescent spectrum of a InGaN-based near-UV LED chip (395 nm) comprising of a mixture of  $\text{Sr}_5(\text{PO}_4)_3\text{Cl}:\text{Eu}^{2+}$ , green-emitting  $(\text{Ba},\text{Sr})_2\text{SiO}_4:\text{Eu}^{2+}$  and red-emitting  $\text{CaAlSiN}_3$  phosphors driven by a current of 350 mA and a voltage of 3.29 V. The inset shows the photo of the fabricated w-LEDs package.

**Tables:****Table 1**

Sr <sub>5</sub> (PO <sub>4</sub> ) <sub>3</sub> Cl		
Crystal system	hexagonal	
Space group	P 63/m	
Z	2	
Cell ratio	$a/b = 1.0000$ $b/c = 1.3682$ $c/a = 0.7309$	
Lattice Parameters	Experiment	Theory
$a$ (Å)	9.8590	9.9957
$c$ (Å)	7.2060	7.2737
$V$ (Å <sup>3</sup> )	606.58	629.38

**Table 2**

R1	R2	R3	R4	R5	R6	R7	R8	R9	R10	R11	R12	R13	R14	R <sub>a</sub>
99	97	96	93	98	97	91	85	63	94	91	94	96	97	94.65

**Table 3**

Phosphor	Excitation wavelength (nm)	Emission peak (nm)	Internal QE (%)
$\text{Sr}_5(\text{PO}_4)_3\text{Cl}:\text{Eu}^{2+}$	395	444	80.53
$\text{KMg}_4(\text{PO}_4)_3:\text{Eu}^{2+6}$	365	450	50.44
$\text{RbBaPO}_4:\text{Eu}^{2+48}$	380	430	79.80
$\text{Sr}_3\text{MgSi}_2\text{O}_8:\text{Eu}^{2+48}$	380	455	78.30
$\text{BAM}:\text{Eu}^{2+6,33}$	365	462	88.99

Figures:

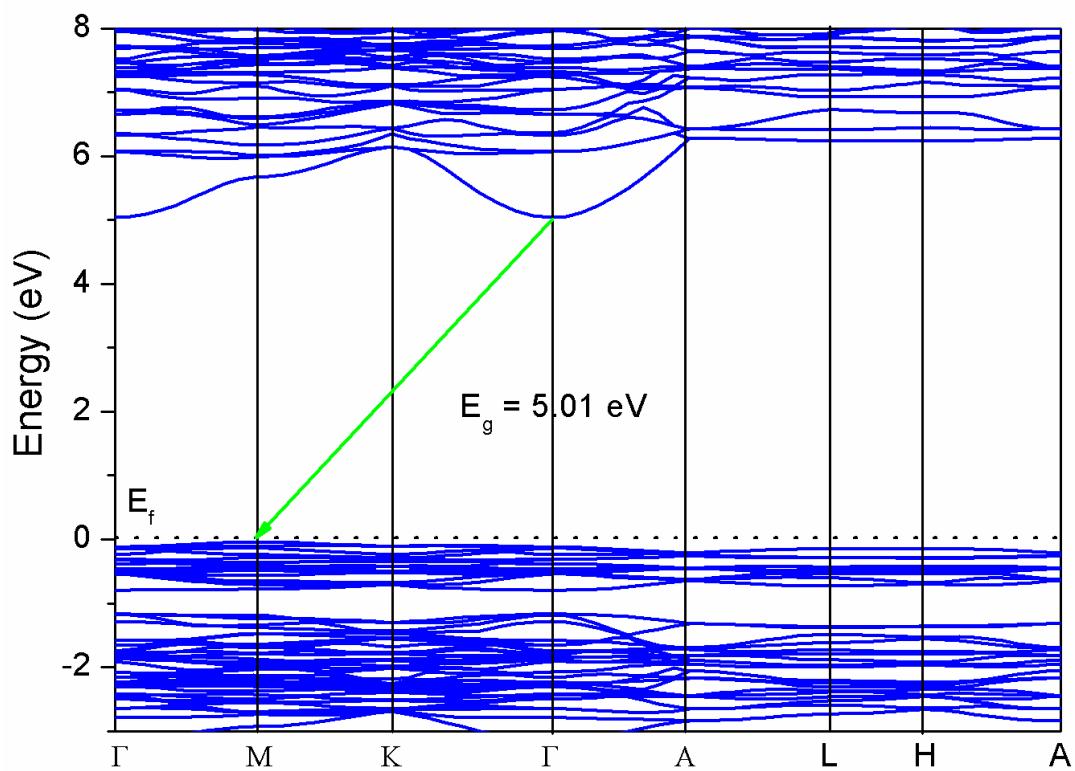


Figure 1

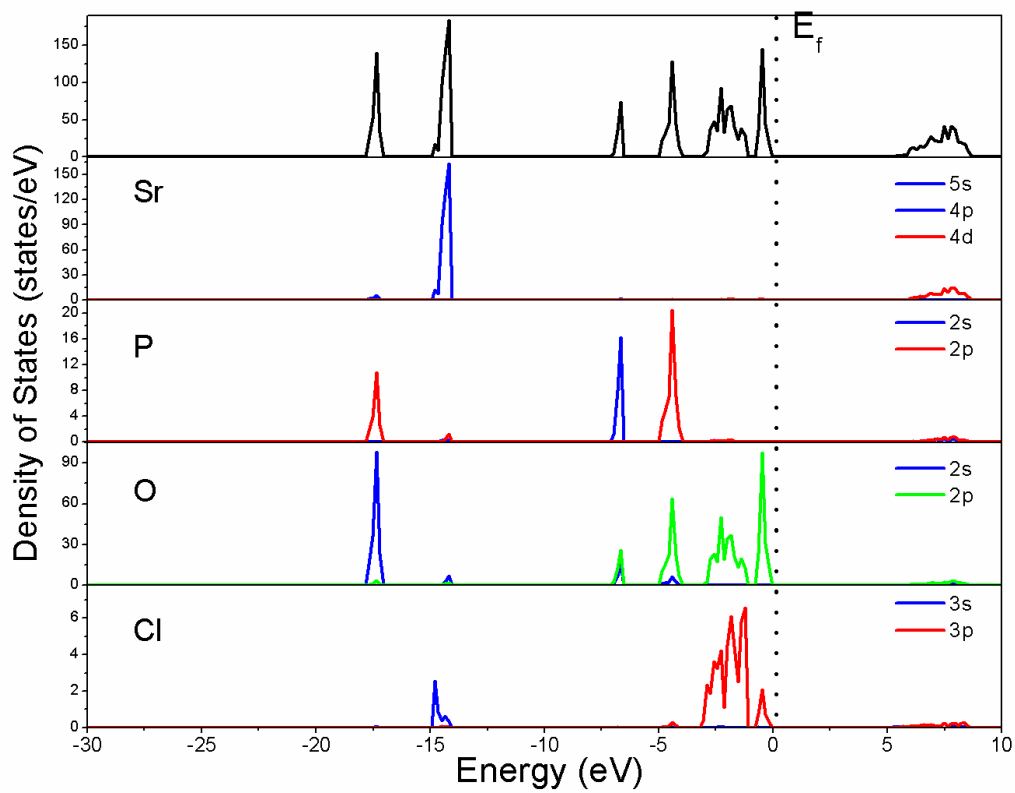


Figure 2

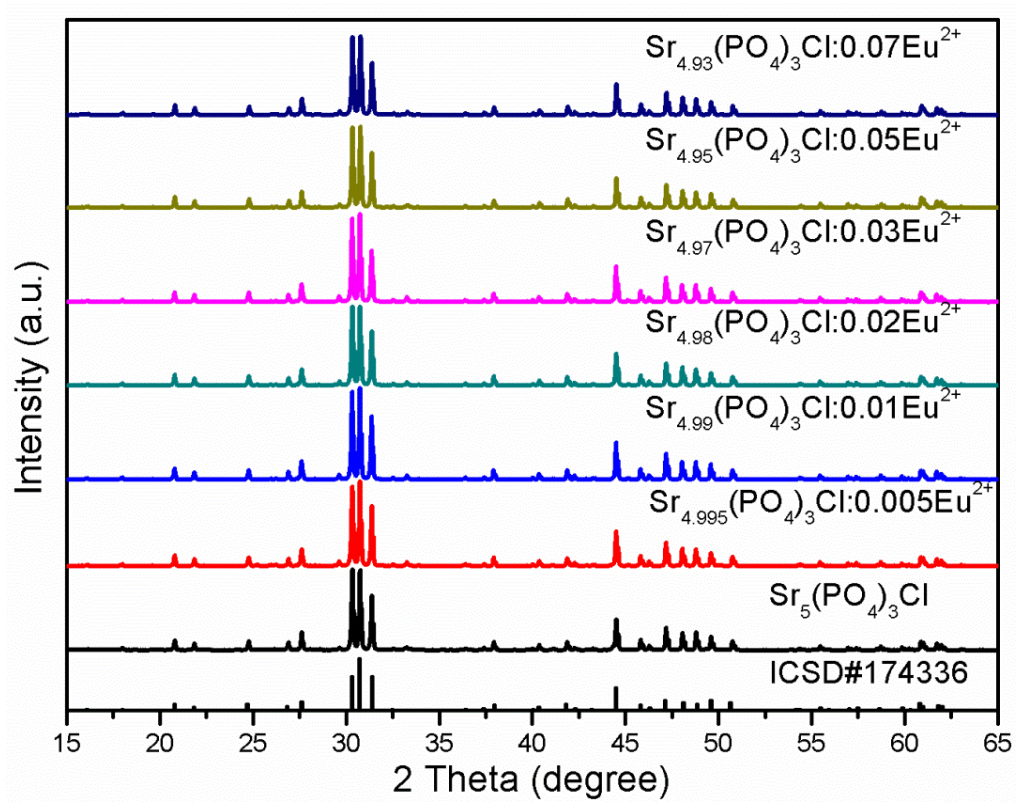


Figure 3

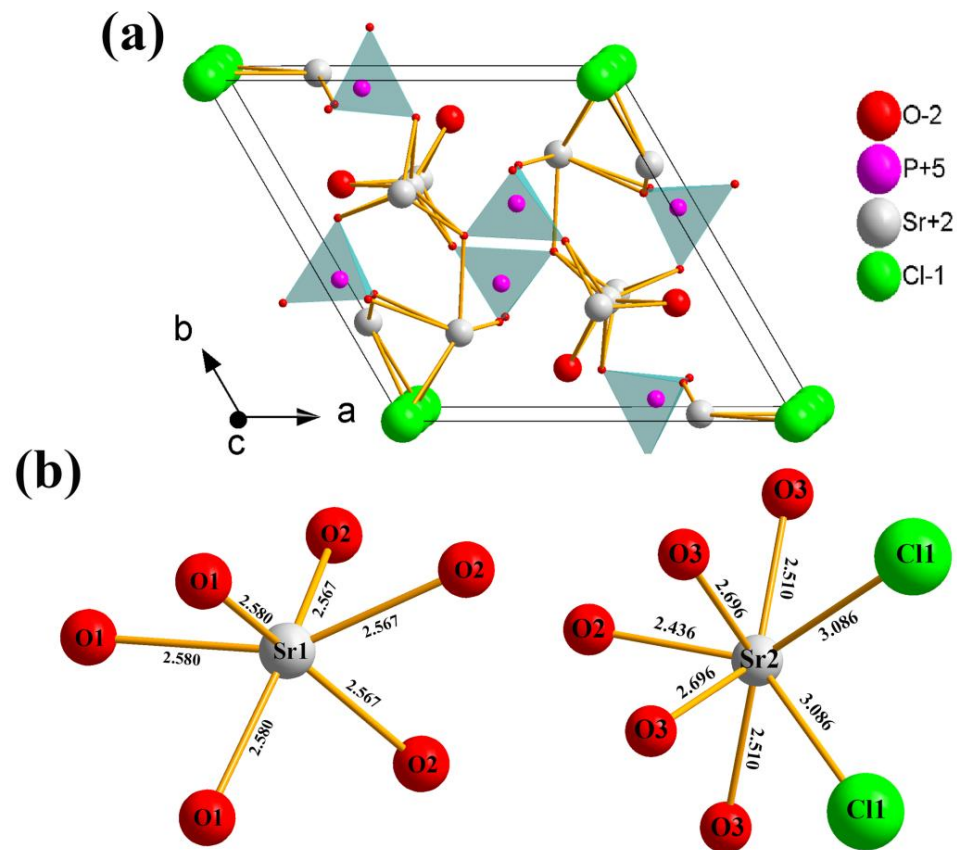


Figure 4

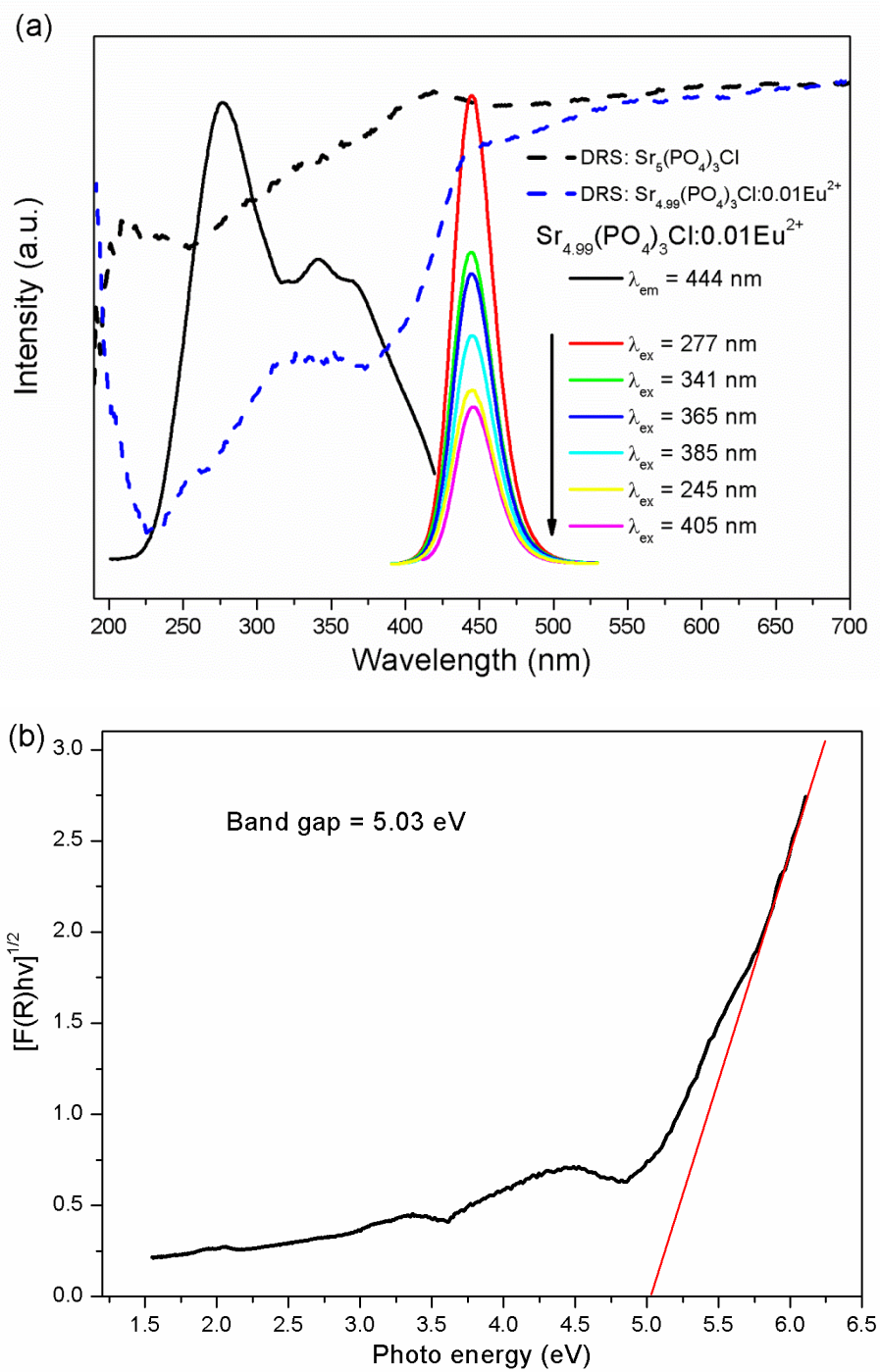


Figure 5

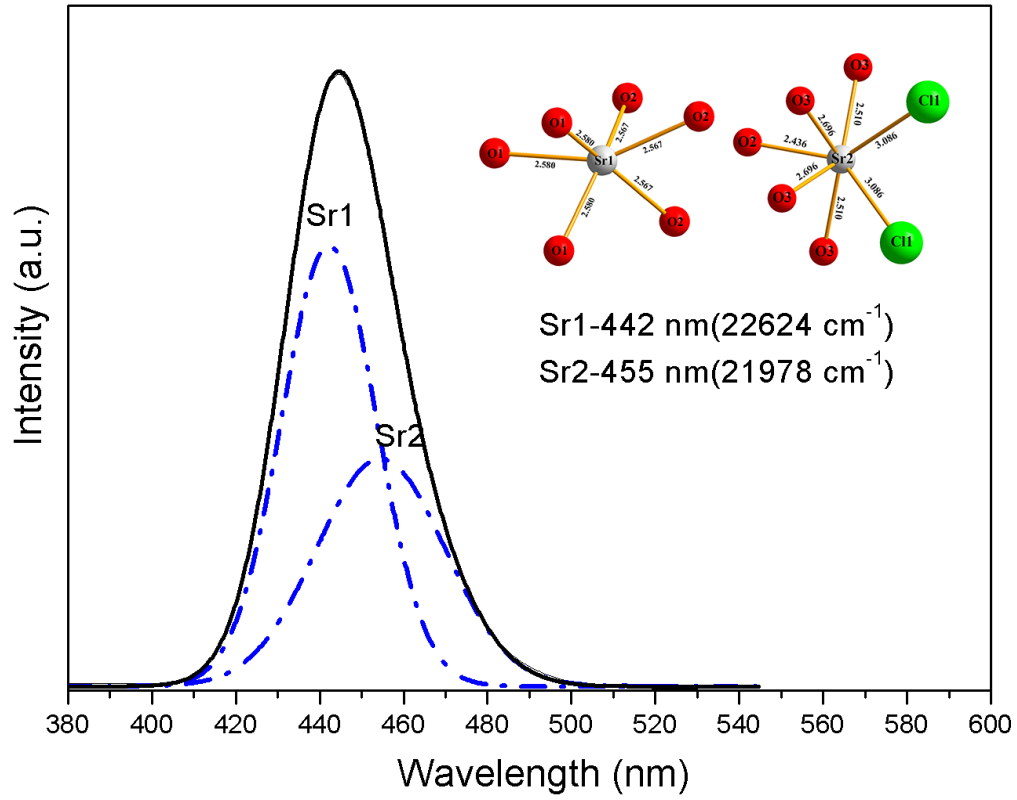


Figure 6

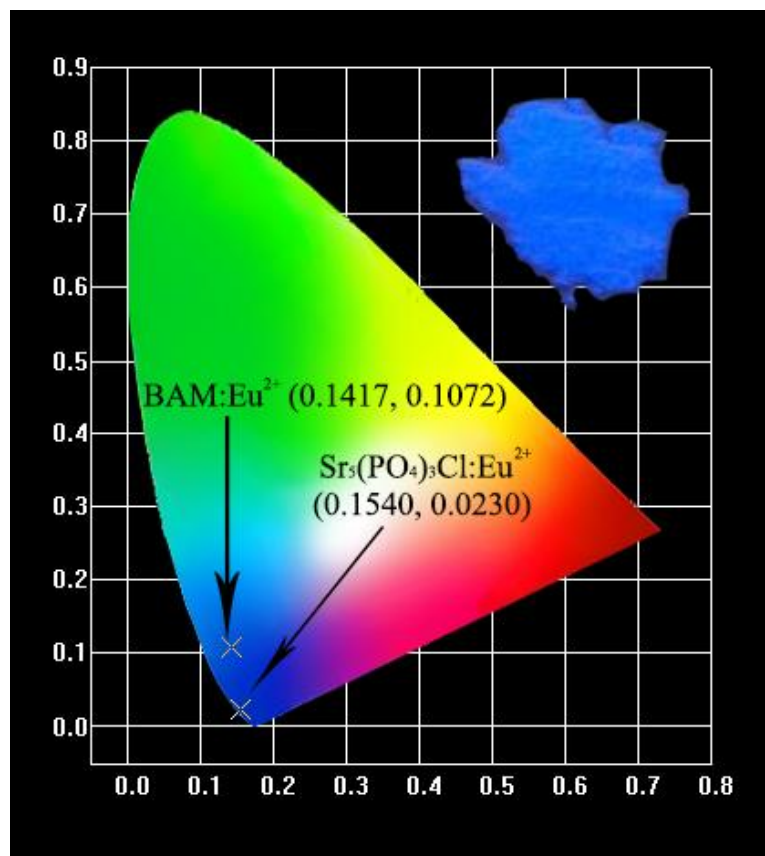


Figure 7

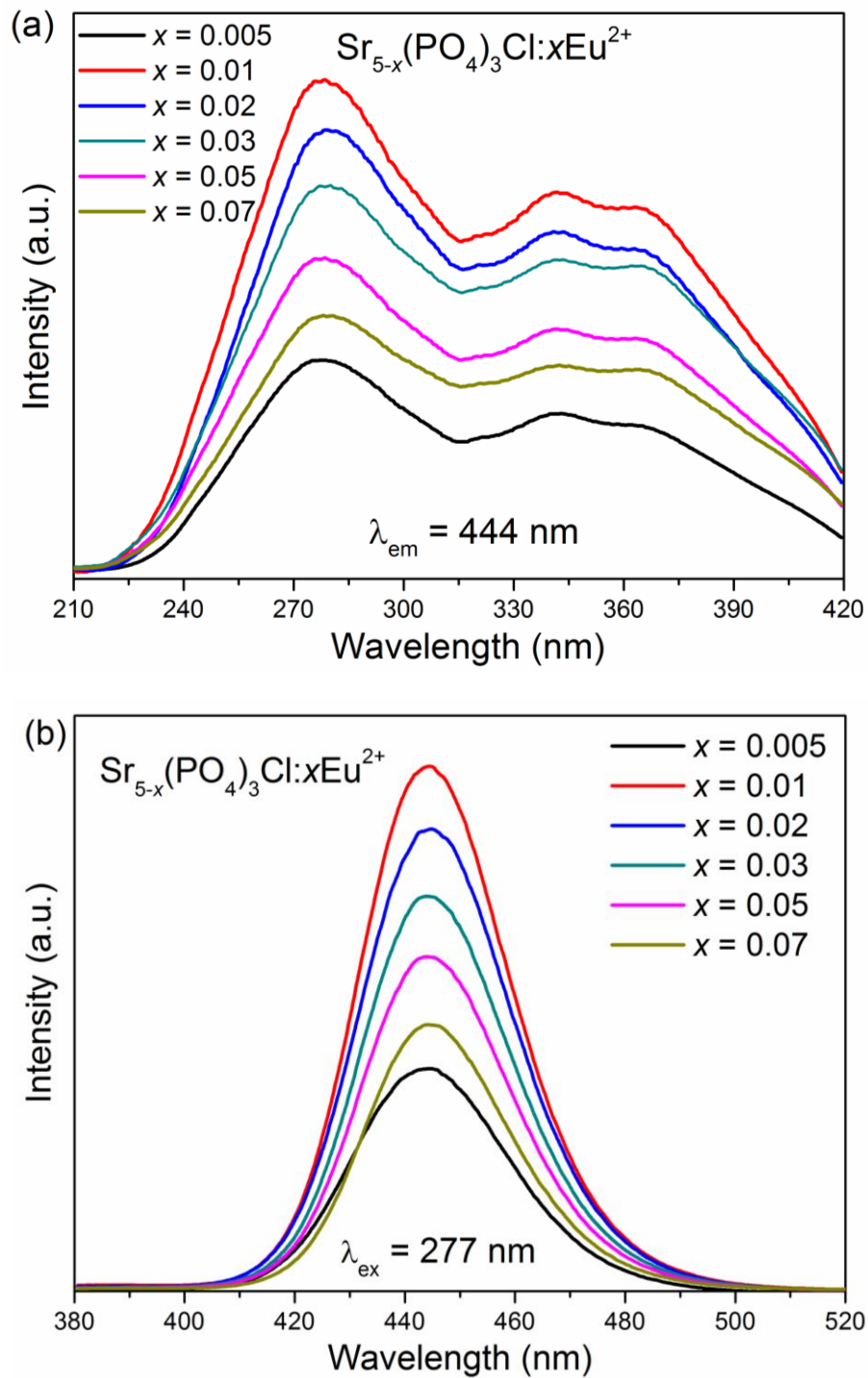


Figure 8

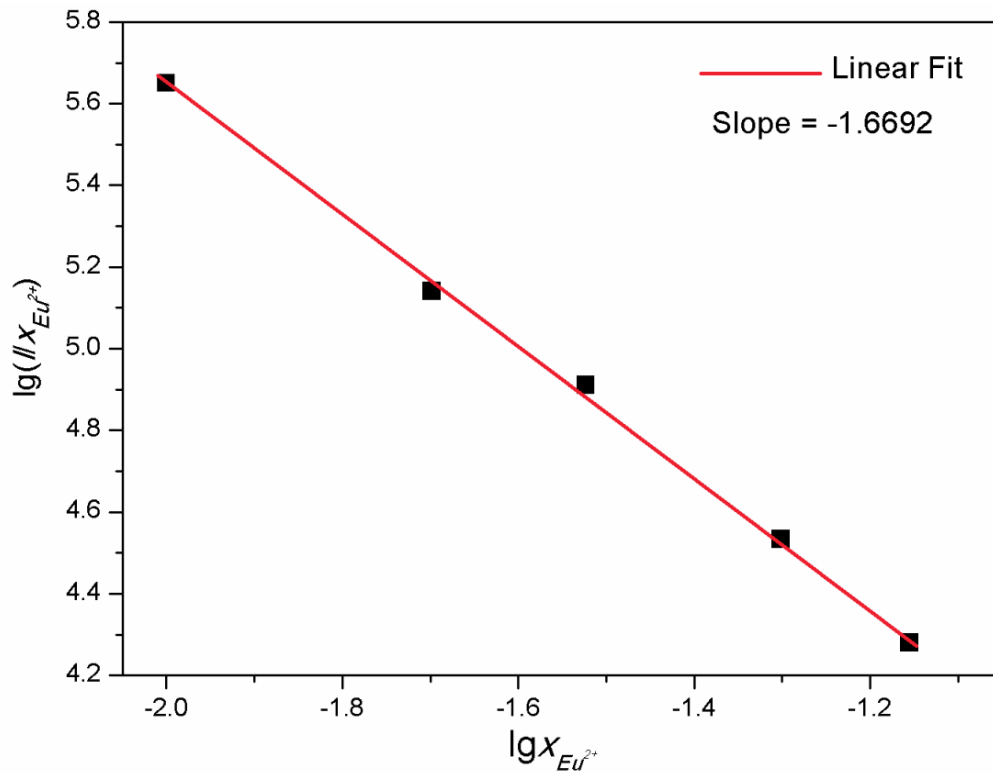


Figure 9

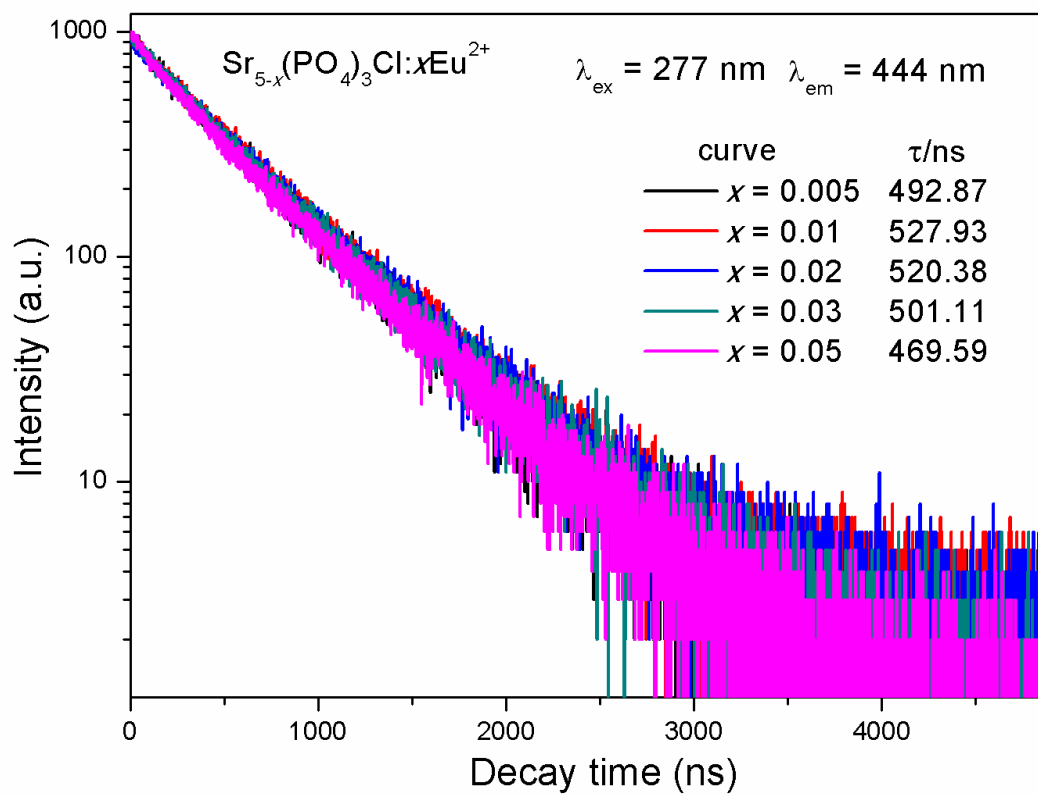


Figure 10

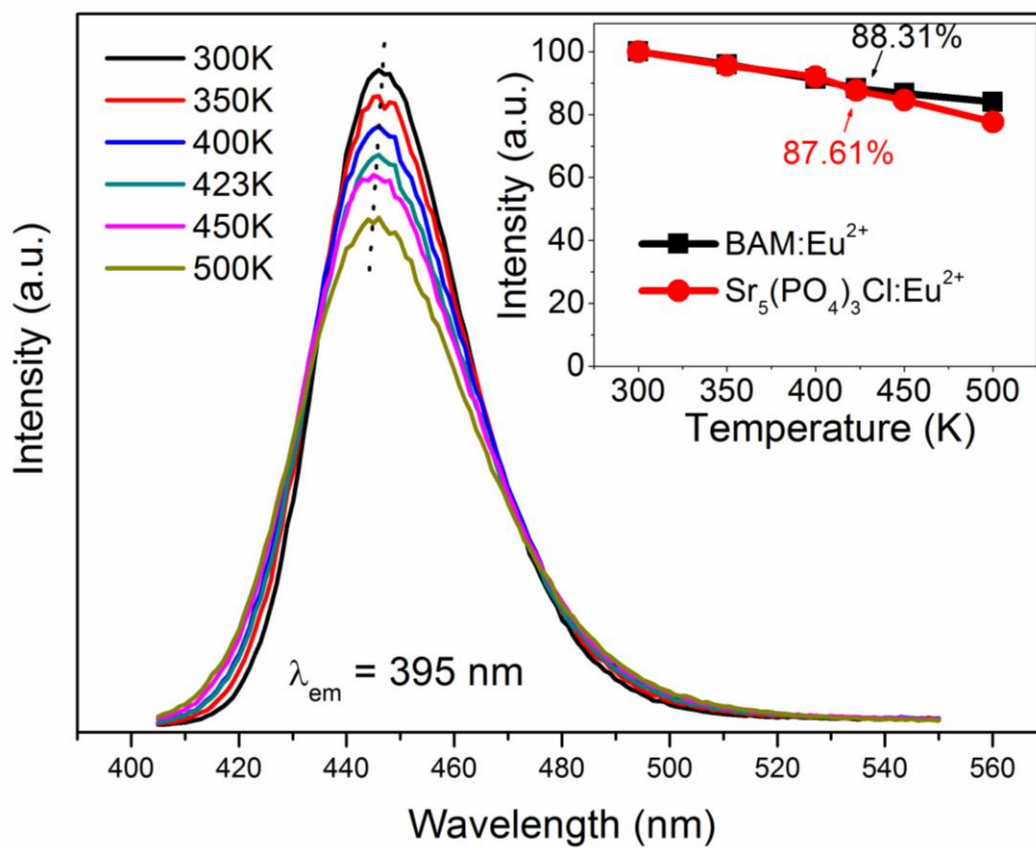


Figure 11

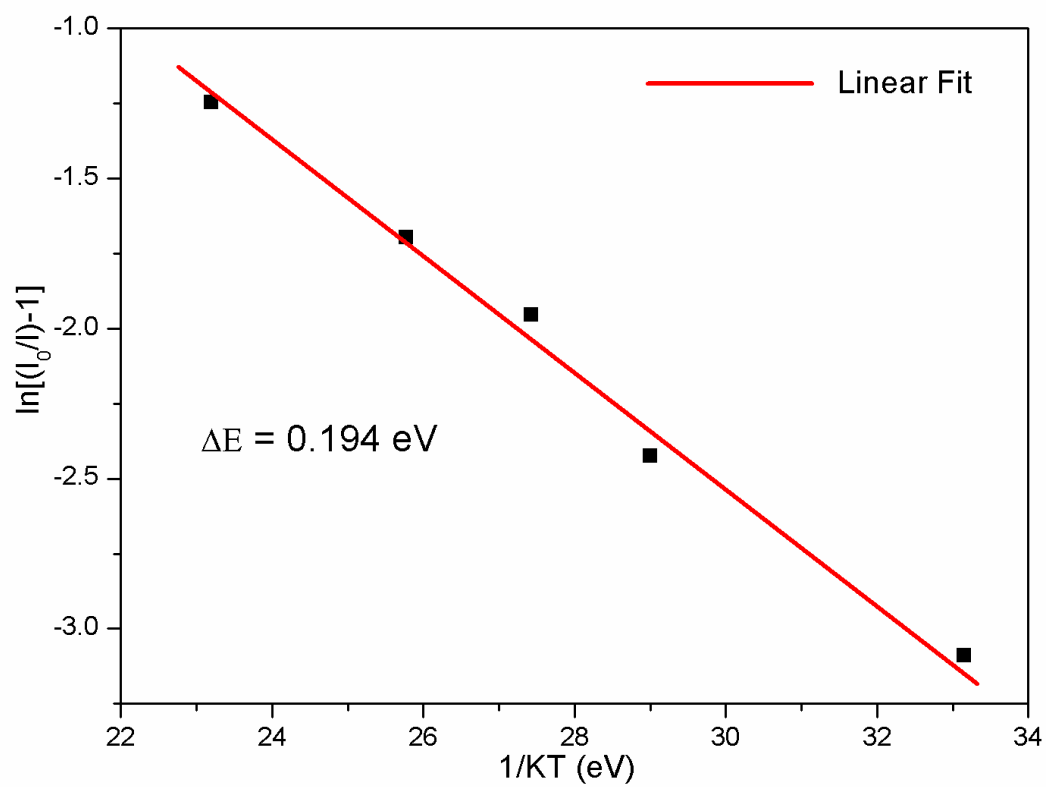


Figure 12

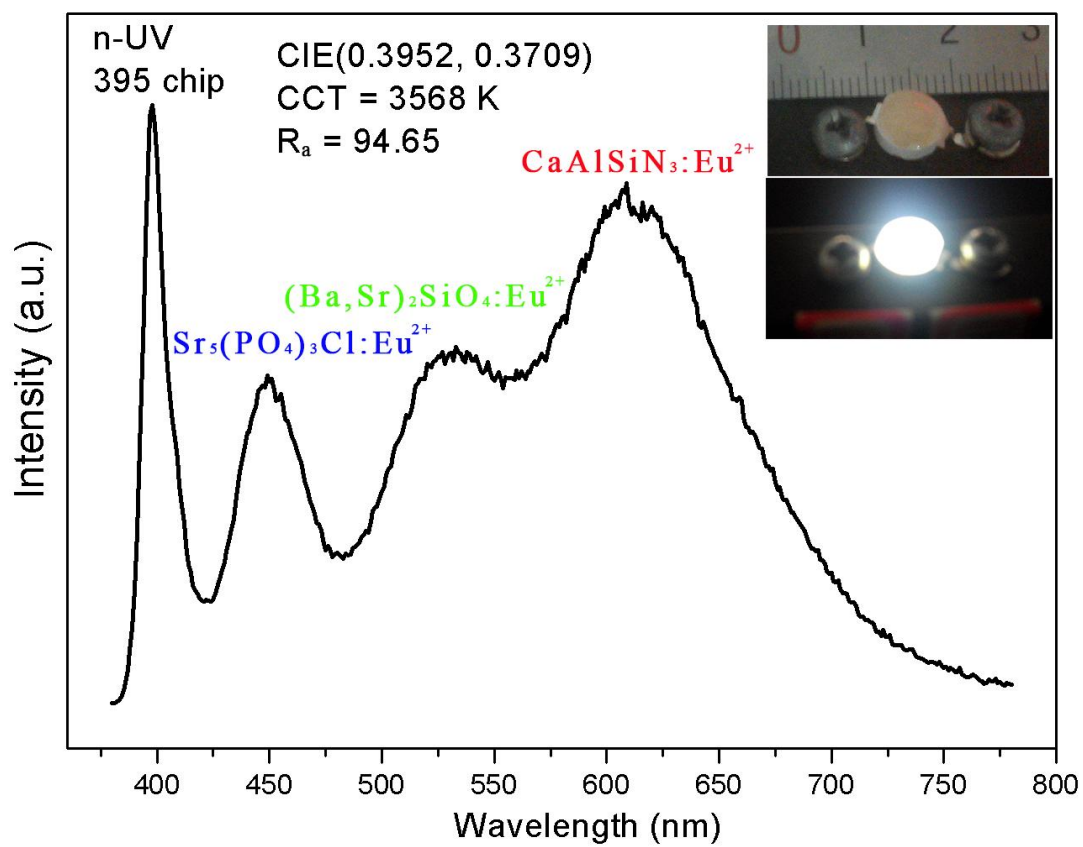


Figure 13